

**Peptide Self-Assembly**

# Dynamic Control of Cyclic Peptide Assembly to Form Higher-Order Assemblies

Chongyang Wu, Hongyue Zhang, Nan Kong, Bihan Wu, Xinhui Lin, and Huaimin Wang\*

**Abstract:** Chirality correction, asymmetry, ring-chain tautomerism and hierarchical assemblies are fundamental phenomena in nature. They are geometrically related and may impact the biological roles of a protein or other supermolecules. It is challenging to study those behaviors within an artificial system due to the complexity of displaying these features. Herein, we design an alternating D,L peptide to recreate and validate the naturally occurring chirality inversion prior to cyclization in water. The resulting asymmetrical cyclic peptide containing a 4-imidazolidinone ring provides an excellent platform to study the ring-chain tautomerism, thermostability and dynamic assembly of the nanostructures. Different from traditional cyclic D,L peptides, the formation of 4-imidazolidinone promotes the formation of intertwined nanostructures. Analysis of the nanostructures confirmed the left-handedness, representing chirality induced self-assembly. This proves that a rationally designed peptide can mimic multiple natural phenomena and could promote the development of functional biomaterials, catalysts, antibiotics, and supermolecules.

## Introduction

Supramolecular nanotubular structures formed by proteins are prevalent within biological membranes, which can facilitate intercellular communication and pathology detection.<sup>[1]</sup> To fulfill the various biological functions, the dynamic high-order assemblies (e.g., tertiary structures) of proteins are the prerequisite requirement.<sup>[2]</sup> Inspired by nature, synthetic nanotubular structures via a dynamic covalent linkage (or stimuli-responsive linkage) have drawn considerable attention from scientists with applications in

ion channels,<sup>[3]</sup> sensors,<sup>[4]</sup> nanomedicine,<sup>[5]</sup> and drug delivery.<sup>[6]</sup> Peptides with charged amino acids (i.e., Glu, Asp, Lys, Arg) are a class of pH-responsive materials due to the reversible protonation or deprotonation processes.<sup>[7]</sup> However, the dynamic control of transformation between a linear peptide and the corresponding cyclic peptide by employing a reversible linkage has shown great potential in medicinal therapy and supramolecular chemistry,<sup>[8]</sup> which has been less explored.

Cyclic peptides are widely used building blocks to access synthetic nanotubes,<sup>[9]</sup> because the backbones of peptides can provide multiple intermolecular hydrogen bond donors and acceptors. Pioneered by Ghadiri et al.,<sup>[10]</sup> cyclic peptides with alternating D,L amino acids in an even number of residues could self-assemble to form nanotubular structures, and substantial examples have shown the modification of this class of cyclic peptides and their diverse applications in various fields (i.e., antibiotics, drug delivery, etc.)<sup>[9h,11]</sup> However, the poor solubility of nanotubes in water caused by the aggregates prohibits the further application of cyclic peptides.<sup>[10]</sup> Thus, the design of cyclic peptides with a strong propensity to assemble without compromising the solubility in water remains challenging. Intriguingly, head-to-tail cyclization through a reversible imine linkage catalyzed by an unusual NAD(P)H-dependent reductase domain has been revealed in certain bacteria.<sup>[12]</sup> However, it is difficult to study the dynamics of a cyclic peptide bridged by an imine in water due to the lability.<sup>[13]</sup> Strategies have been developed recently to construct structurally diverse peptides by trapping imines with various inter- and intramolecular nucleophiles.<sup>[14]</sup> Interestingly, Raj group reported a highly chemoselective “Cyclick” chemistry strategy for the synthesis of cyclic peptides featuring a 4-imidazolidinone ring in the presence of excess DMAP (4-(Dimethylamino)pyridine) in a cosolvent of DMF and water.<sup>[15]</sup> Nevertheless, in-depth studies to resolve the thermodynamics in cyclization and the assembly behaviors in water are still in urgent need.

So far, most of the reported work of cyclic peptides produced via an irreversible amide coupling reaction, featuring a symmetrical backbone<sup>[16]</sup> self-assemble to form 1D nanotubular structures and even 2D nanosheets<sup>[17]</sup> (Figure 1a). Studies mainly focus on the modifications of nanotubes via a reversible covalent linkage through peptide side chains.<sup>[9b,e,18]</sup> However, the self-assembly (SA) behaviors and the conformational tuning diversity of cyclic peptides with an asymmetrical backbone, such as incorporating a heterocycle has been less explored. Therefore, new strategies toward constructing structurally and functionally diverse cyclic peptides are still in urgent need of

[\*] Dr. C. Wu, H. Zhang, N. Kong, B. Wu, X. Lin, Prof. Dr. H. Wang  
 Key Laboratory of Precise Synthesis of Functional Molecules of Zhejiang Province, Department of Chemistry, School of Science, Westlake University, Institute of Natural Sciences, Westlake Institute for Advanced Study  
 No. 600 Dunyu Road, Hangzhou 310024, Zhejiang Province (China)  
 E-mail: wanghuaimin@westlake.edu.cn  
 Prof. Dr. H. Wang  
 Westlake Laboratory of Life Sciences and Biomedicine, School of Life Sciences, Westlake University  
 Hangzhou, 310024  
 Zhejiang (China)

supramolecular chemistry. This work reports the dynamic control of self-assembly of the asymmetrical cyclic peptides to form higher-order nanostructures in an aqueous solution (Figure 1b). We design and synthesize cyclic monomers from partially epimerized linear peptides at neutral pH, the resulting cyclic peptides are coincidentally with the 4-imidazolidinone-fused peptides reported by Raj et al.<sup>[15]</sup> Such modifications not only provide accesses to investigate the thermodynamics of a ring-chain tautomerism in water by changing the pH, but also provide a platform to evaluate the self-assembly diversity. The cyclization of which leads to two diastereomers for most linear peptides. The major isomer displays strong resistance to ring-opening under thermal conditions at neutral pH. In contrast, the minor isomer could transform into the major isomer via a plausible ring-opening and spontaneous cyclization mechanism. The ring-chain tautomerism and self-assembly morphology cycles could be tuned by simply changing the pH, followed by a standard annealing process. The resulting cyclic peptide initiates the 1D to 2D assembly and further self-assemble to form left-handed coils. Both time-dependent transmission electron microscopy (TEM) and atomic force microscopy (AFM) studies illustrate the assembly evolution, from 1D nanoribbon arrays to intertwined hierarchical nanostructures. This study provides an alternative strategy to design reversible higher-order assemblies of the asymmetrical cyclic peptides.

## Results and Discussion

### Monomer Design and Characterization

Reversible imine linkage has been found in naturally occurring cyclic peptides (i.e., Nostocyclopeptides<sup>[19]</sup>). The reversible cyclization leads to a stereochemically pure cyclic peptide with a partially epimerized C-terminus.<sup>[14,19b,20]</sup> However, the dynamics of a cascade imine/nucleophilic addition in a structurally diverse D,L peptide with a C-terminal epimer remains unknown, although the ring-chain tautomerism in oxazolidine,<sup>[21]</sup> thiazolidine,<sup>[22]</sup> imidazolidinone<sup>[23]</sup> has been characterized in small molecules. The previous study indicated that the appropriately designed cyclic amphiphilic peptide could undergo a transition from 1D nanotubes to 2D nanosheets reversibly.<sup>[17a]</sup> We hypothesized that inserting a heterocycle with five or six atoms into an alternating D,L-cyclic peptide to form an asymmetrical cyclic peptide could alter their planar ring conformation and result in hierarchical higher-order assemblies. The designed cyclic peptide in this work is based on cascade reactions of aldimine condensation and a nucleophilic addition to the aldimine<sup>[24]</sup> to form a five- or six-membered ring (Figure 2a).<sup>[14]</sup> An amphiphilic peptide  $\text{NH}_2\text{-L-Ser-D-Glu-L-Gln-D-Glu-L-Ala-D-Leu-L-Trp-D-Leu-H}$  (**1**) (Figure 2a) modified from literature<sup>[17a]</sup> was synthesized, containing a D-Leu-H at the C-terminus. The region-specific ligation reaction could occur under mild conditions in water without side chain protecting groups, extra coupling reagents and base. The cyclization occurs slowly at room temperature (pH 7.4) but

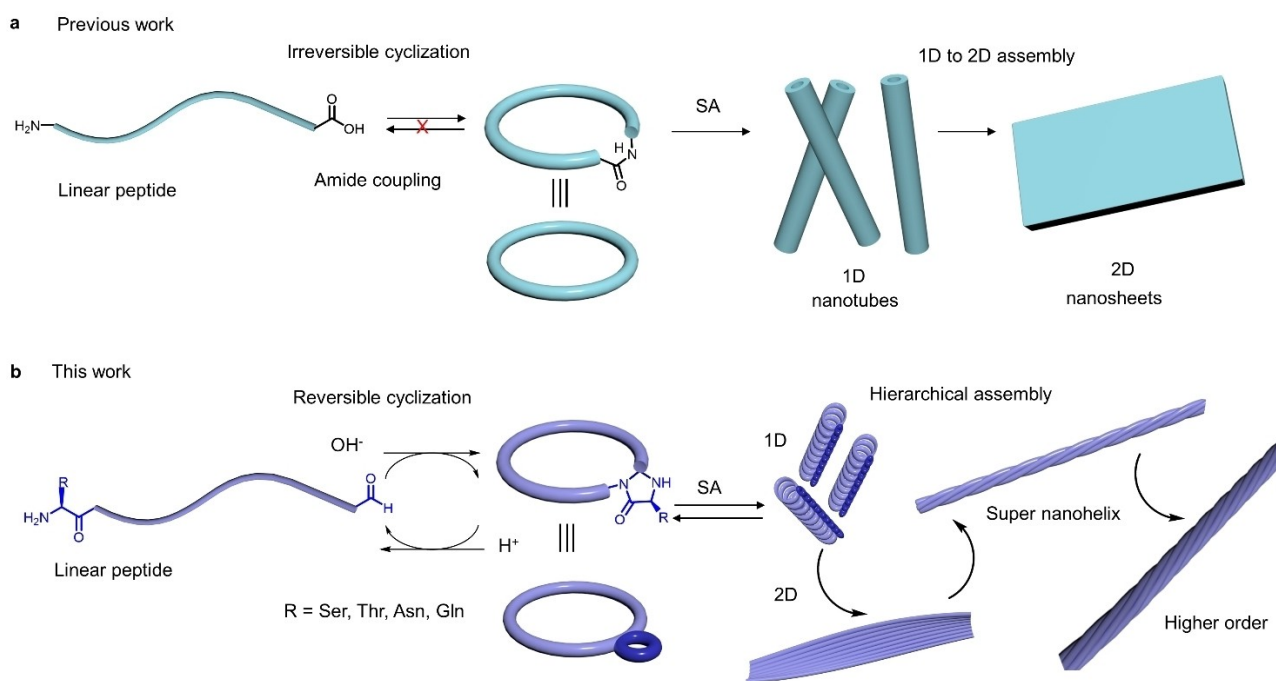


**Figure 1.** Schematic illustration of the irreversible and reversible cyclization and the assembly of the cyclic monomers. a) Irreversible cyclization of the linear peptide through an amide bond formation, and the assembly of cyclic monomers to form 1D nanotubes and 2D nanosheets. b) Thermal-induced reversible cyclization of a cyclic D,L peptide with an asymmetrical backbone and the spontaneous assembly to form intertwined hierarchical nanostructures in water. Neutral or slightly basic conditions favor for the cyclization, while acidic conditions induce ring-opening.

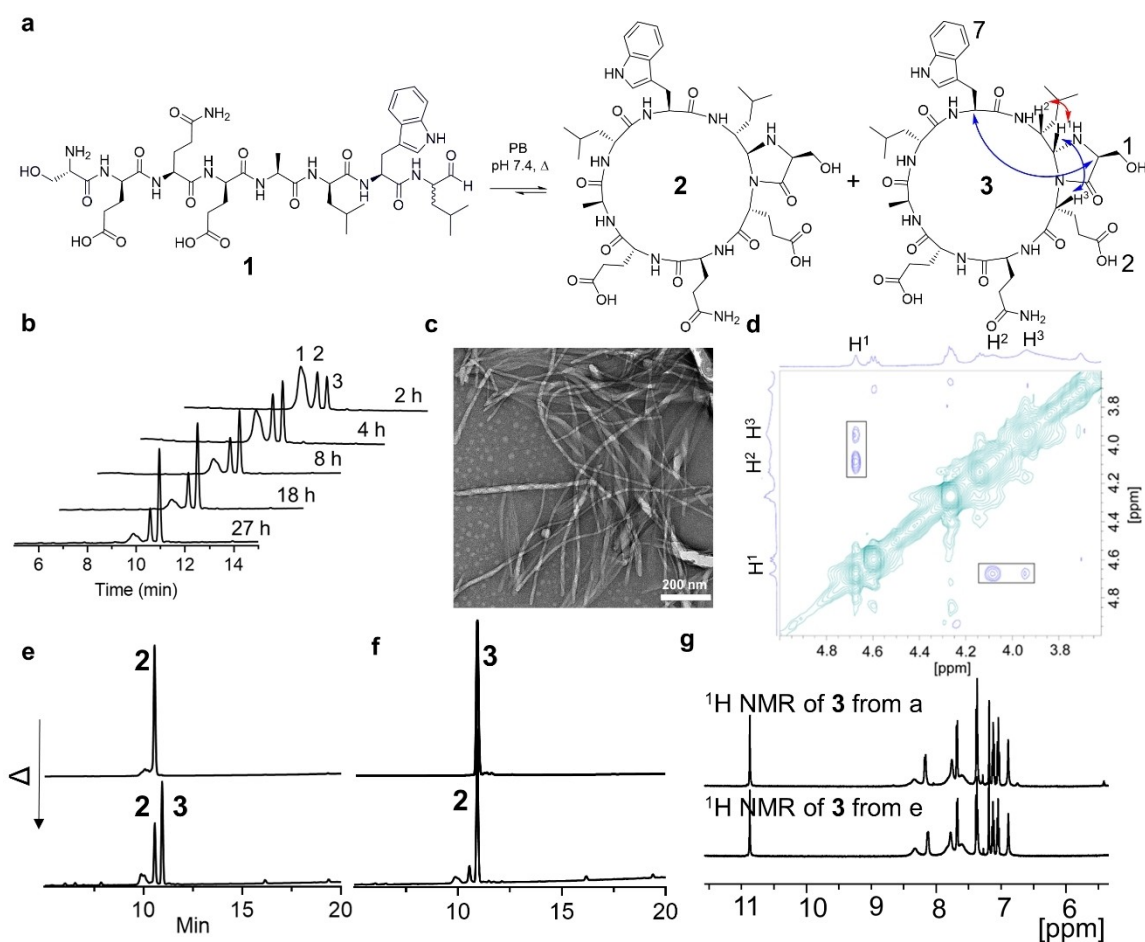


**Figure 2.** Characterization of the peptide cyclization. a) Reversible cyclization of an octapeptide via a cascade imine/4-imidazolidinone formation. Key ROEs are labeled with double arrows (red for strong ROE, blue for weak ROE; 1, 2 and 7 indicate the residue numbers in the sequence). b) Reaction progress monitored by RP-HPLC. c) TEM images of the reaction mixture indicative of assembly. d) Partial 2D ROESY spectrum (600 MHz, 298 K, DMSO- $d_6$ ) of **3** showing the cross peaks between  $H^1$  and  $H^2/H^3$ . e, f) HPLC analysis of the thermoreversibility. e) The isolated cyclic peptide isomer **2** was resuspended in buffer at pH 7.4, incubated at 68 °C for 48 h. f) The isolated cyclic peptide isomer **3** was resuspended in buffer at pH 7.4, incubated at 68 °C for 48 h. g)  $^1H$  NMR spectra comparison of **3** obtained from the cyclization reaction (a) and isomerization of **2** (e), respectively.

significantly high at elevated temperature. The cyclization leads to a pair of diastereomers **2** and **3** with a diastereomeric ratio (dr) 1:3, which can be separated to afford the major diastereomer by RP-HPLC (Figure 2a, 2b).

The linear peptide consists of a dominant C-terminal D-aldehyde (80%) and a C-terminal epimer (L, 20%) being inseparable and appears as a broad peak even in analytical RP-HPLC. The cyclization conversion to **3** was slightly lower than **2** at 2 h but exceeded rapidly later (Figure 2b). HPLC results showed that the reaction system almost reached an equilibrium (ratios for each component would not change much) after 27 h with **3** being the dominant component. TEM results revealed the formation of nanoribbon arrays and intertwined nanotubular structures after stabilizing the system for 24 h at room temperature (Figure 2c). To explore the thermostability and the individual contribution to the morphology in the system, we next isolated the isomers by RP-HPLC and evaluated their self-assembly ability. The isomer **2** decreased significantly under

heating at pH 7.4 after 48 h, which transformed to a small amount of **1** (linear) and a large amount of **3** (verified by  $^1H$  NMR, Figure 2e, 2g), indicating the low thermostability of isomer **2**. By contrast, the isomer **3** displayed high thermostability, only a negligible amount of the linear peptide **1** and the cyclic isomer **2** were detected under the same conditions (Figure 2f). These results suggest that the isomer **2** adopts a thermally unfavorable conformation, while **3** locates in a much more stable conformation. We assumed that the conversion of **2** to **3** undergoes a ring-opening reaction, as evidenced by the resulting linear peptide, which spontaneously cyclized to give **2** and **3** (Figure S23). To investigate the potential self-correcting mechanism during cyclization, we synthesized a linear peptide ( $NH_2$ -L-Ser-D-Glu-L-Gln-D-Glu-L-Ala-D-Leu-L-Trp-L-Leu-H, **1'**) with a C-terminal L-configured aldehyde (90%), albeit with a D-configured epimer (10%) (Figure S1). Surprisingly, this peptide showed a similar conversion as **1** to afford a pair of cyclic diastereomers (**2'** and

3') with a ratio of 1:3.2 after 48 h (Figure S2, S3). Detailed 1D, 2D NMR spectra and circular dichroism (CD) spectra for this pair of cyclic isomers (2' and 3') showed the identical structural information as for 2 and 3, respectively (Figure 2g and S4–6, 24).

Therefore, we proposed that the C-terminal aldehyde may undergo a rapid epimerization from L- to D-configuration prior to the spontaneous cyclization, which is consistent with the finding in the synthesis of Nostocyclopeptides.<sup>[20]</sup> 2D NMR spectrum of cyclic 3 indicated the chirality of the newly formed chiral center. The strong ROE cross-peak between H<sup>1</sup> and H<sup>2</sup> and weak ROE between H<sup>1</sup> and H<sup>3</sup> confirmed a *cis* conformation of H<sup>1</sup> and H<sup>2</sup> in 3 (Figure 2a, 2d, S18). The weak ROE signals between H<sup>1</sup> and H<sup>3</sup>, H<sub>u7</sub> and H<sub>u1</sub> could be attributed to a turn conformation induced by the 4-imidazolidinone ring.<sup>[15a]</sup> However, we could hardly observe any characteristic ROE signals abovementioned for isomer 2, which prevented the actual assignment of the conformation (Figure S7). Nevertheless, considering the rapid epimerization of L- to D-configured aldehyde prior to cyclization, we suspected that

the isomer 2 having a opposite chirality in the conjugation site compared to 3 (Figure S8).

Temperature-dependent CD results showed that the freshly prepared solution of 3 (100 μM) in phosphate buffer (pH 7.4) exhibited two positive peaks at 208 nm and 222 nm (Figure 3c), respectively, indicating a left-handed helix that is different from general beta sheet conformation adopted by alternating D,L cyclic peptides. The distinct helical features might be stabilized by intramolecular hydrogen bonds (*i, i+4*) and *n*→*π*\* interactions within a rigid cyclic scaffold.<sup>[25]</sup> The intensity of positive peaks decreased with the increase of temperature, suggesting the destabilization of the secondary structure at elevated temperatures. The secondary structure could be recovered after cooling to the initial temperature (20 °C) (Figure 3c and S9). Despite the decreased intensity along with increased temperature, CD signal was preserved across the thermal annealing processes, suggesting the peptide conformation did not change significantly.

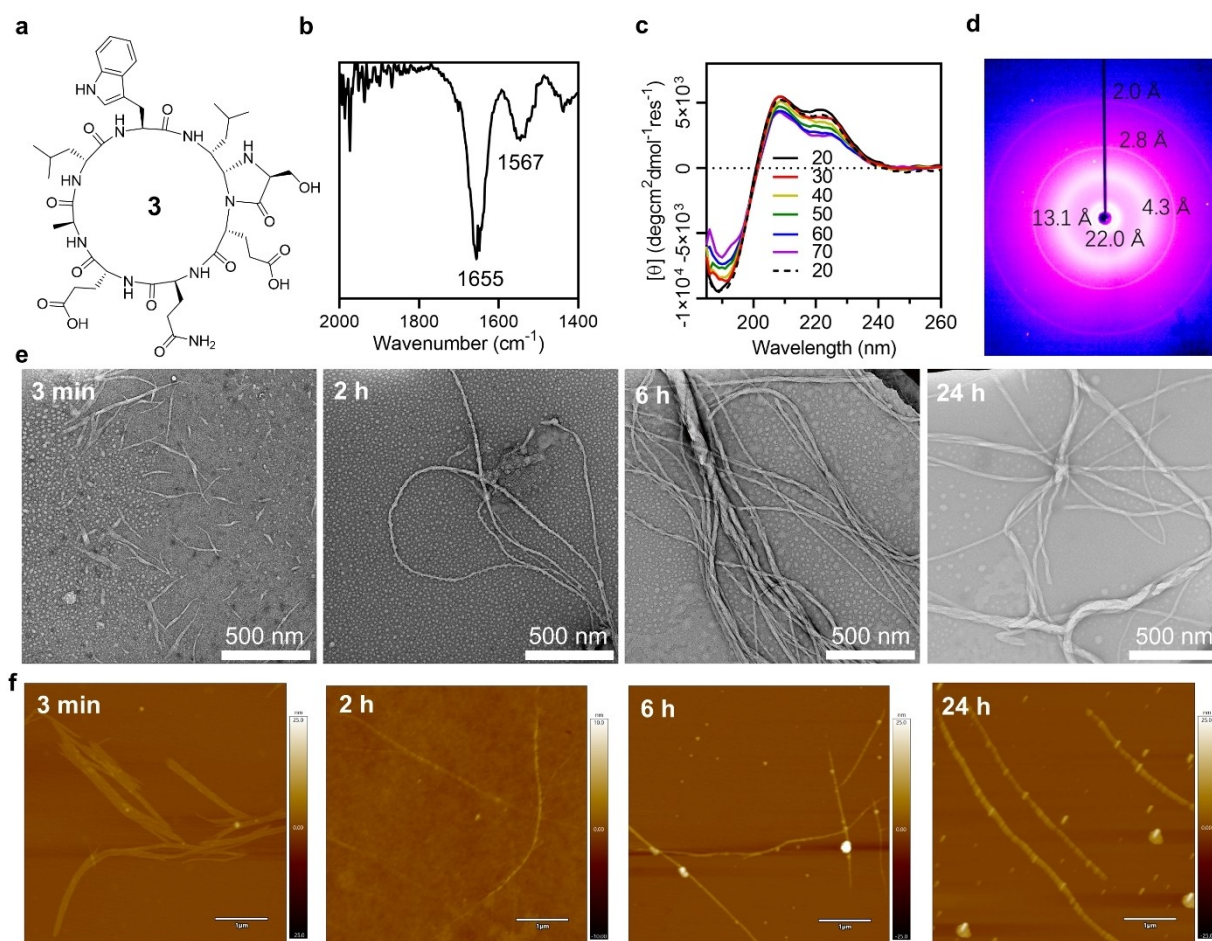


**Figure 3.** Structural characterization of 3. a) Chemical structure of 3. b) Partial FT-ATR spectrum of dried nanostructures of 3. c) Temperature-dependent CD spectra of 3 (100 μM) in 10 mM phosphate buffer (pH 7.4), from 20 °C to 70 °C (solid line) and returned to 20 °C (dashed black line) finally. d) Wide angle X-ray scattering (WAXS) profile of a dry sample of nanostructures of 3, showing the internal distances in the nanostructures. e) TEM images showing the time-dependent assembly of 3 in aqueous media at pH 7.4. f) AFM images showing the assembly evolution from 3 min to 24 h.

### Characterizations of the Nanostructures

The isomer **3** showed a strong propensity to form intertwined or braided nanostructures in a wide range of concentrations from 0.5 mM to 6 mM, with no significant concentration-dependent differences for the length and diameters (Figure S10). The largest diameter for some coils even could reach 80 nm (Figure S11). The nanostructures being dominant left-handed filament bundles displayed good flexibility with length reaching several micrometers. Scanning electronic microscopy (SEM) confirmed the left-handed chirality (Figure S12), which could be ascribed to the left-handed helical conformation adopted by the monomers. Time-dependent TEM showed that isomer **3** formed nanoribbon-like arrays<sup>[26]</sup> rapidly and then transformed into intertwined nanostructures within 10 min (Figure 3e and S13). The fast assembly process was also recorded by AFM, which displayed a gradual height increase from 3 nm to 6 nm along with the morphology change (Figure 3f, S14). Besides, we also found that the intertwined morphology even can exist in a relatively short length (Figure S15). Interestingly, a recent study on the assembly of covalent organic tubes showed that the formation of intertwined structures attributed to the rapid increase in the length of covalent organic tubes.<sup>[27]</sup> We speculated that the five-membered ring within the cyclic backbone could trigger the formation of intertwined nanofibers without reaching a necessary length due to the left-handedness of the monomer. FT-ATR analysis showed an N–H stretching band at 3279 cm<sup>-1</sup>, and the characteristic amide I band at 1655 cm<sup>-1</sup>, amide II band at 1567 cm<sup>-1</sup> (Figure 3b and S16). As amide I region is more sensitive to peptide conformation, the sharp signal at 1655 cm<sup>-1</sup> is consistent with the helical conformation<sup>[28]</sup> and revealed by CD spectra. The stark conformation difference between **3** and classical cyclic peptides with alternating chirality reveals the incorporation of a 4-imidazolidinone ring may alter the flat conformation adopted by cyclic D,L peptides.<sup>[10]</sup> Wide-angle X-ray scattering was used to probe the internal structure of the dried suspension of hierarchical nanostructures (Figure 3d and S17). The signal at 2.00 Å and 2.80 Å suggested a strong and weak hydrogen bond in the system. The scattering signals at 4.3 Å can be correlated to the axial spacing between two cyclic monomers along the nanofibers. Further, the two sharp scattering signals at 13.1 Å and 22.0 Å might be correlated to the interspacing of nanofibers and the distance between two 2D intertwined structures, respectively. The scattering signals in this system are slightly lower than the data reported by Montenegro et al. for 2D nanosheets that resulted from 1D nanotubes,<sup>[17a]</sup> implying a similar but more compact packing model in these intertwined nanotubular structures.

### pH-Responsive Self-Assembly Behavior

We next performed the pH-dependent thermostability of cyclic peptide **3** (1 mM) in phosphate buffer at pH 3.0, 5.0, 7.4, and 9.0, respectively. A standard annealing process was applied (at 68 °C for 24 h then return to RT). The thermal

induced reversibility can be observed when lowering the pH from 7.4 to 5.0 and 3.0 (Figure 4a, S19). A significant ring-opening reaction occurred at pH 3.0 to afford the linear peptide (Figure S19). However, the ring-opening reaction was significantly suppressed when the pH value was above 3.0, as evidenced by the relative ratios of the linear peptide in the system. It should be noted that the invisible diastereomer peak at pH 3.0 suggested the inhibition of the ring-closing reaction. These results support that the cyclization reaction is favorable at pHs above 3.0, and the initial cyclic peptide is stable at pH 5.0 to 9.0 even at high temperatures.

TEM images revealed that the cyclic peptide **3** formed intertwined nanotubular structures at pH 7.4 and 9.0 (Figure S20). However, lowering the pH significantly influenced the morphology, as observed at pH 3.0, it mainly formed nanoparticle aggregation together with needle-shaped nanostructures after 1.5 h (Figure 4a, S21). The needle-shaped nanostructures gradually grew into longer fibers, with some forming spindle apparatus-like nanostructures after 24 h. Interestingly, the morphology evolved into intertwined nanostructures after adjusting the pH from 3.0 to 7.4, this is rational since the linear peptide could cyclize again to afford the cyclic diastereomers **2** and **3** under slight basic condition. Although a negligible amount of the linear peptide remained in the system after 24 h, the relative ratios of the components are consistent with the cyclization reaction after reaching the equilibrium (Figure S22). By contrast, at pH 5.0, the monomers tended to form short ribbon arrays after 1.5 h incubation, which further self-assembled to form the intertwined nanostructures after 24 h incubation (Figure 4b). Changing the pH from 5.0 to 7.4 did not affect the intertwined nanostructures.

### Substrate Scope

To investigate the role of the five-membered ring in the cyclic backbone, we synthesized other analogues with different substitutes or six-membered ring. Similarly, the isolated linear peptides with different N-terminal residues in the sequence NH<sub>2</sub>–L–AA–D–Glu–L–Gln–D–Glu–L–Ala–D–Leu–L–Trp–D–Leu–H (AA represents Thr for **4**, Cys for **6**, Asn for **10**, Trp for **12**, respectively) showed a similar epimerization percentage after releasing from the resin followed by purification by RP-HPLC (For characterizations see Figure S29–60). Mostly, they showed an incomplete conversion due to the reversibility, giving two diastereomers after cyclization except peptide **6** and **12**. Because of the high nucleophilicity of the thiol, the cyclization of **6** at RT resulted in a thiazolidine ring fused cyclic peptides with a pair of diastereomers being inseparable by RP-HPLC rather than 4-imidazolidinone fused cyclic peptide (Figure S38). Besides, the linear peptide **12** (with N-terminal Trp) showed a nearly quantitative conversion to the cyclic peptides (**13**, major isomer) as monitored by RP-HPLC after 13 h incubation at room temperature via the Pictet–Spengler reaction (Figure S55). Compound **13** has a calculated yield reaching 75 % in RP-HPLC, while the other three diaster-

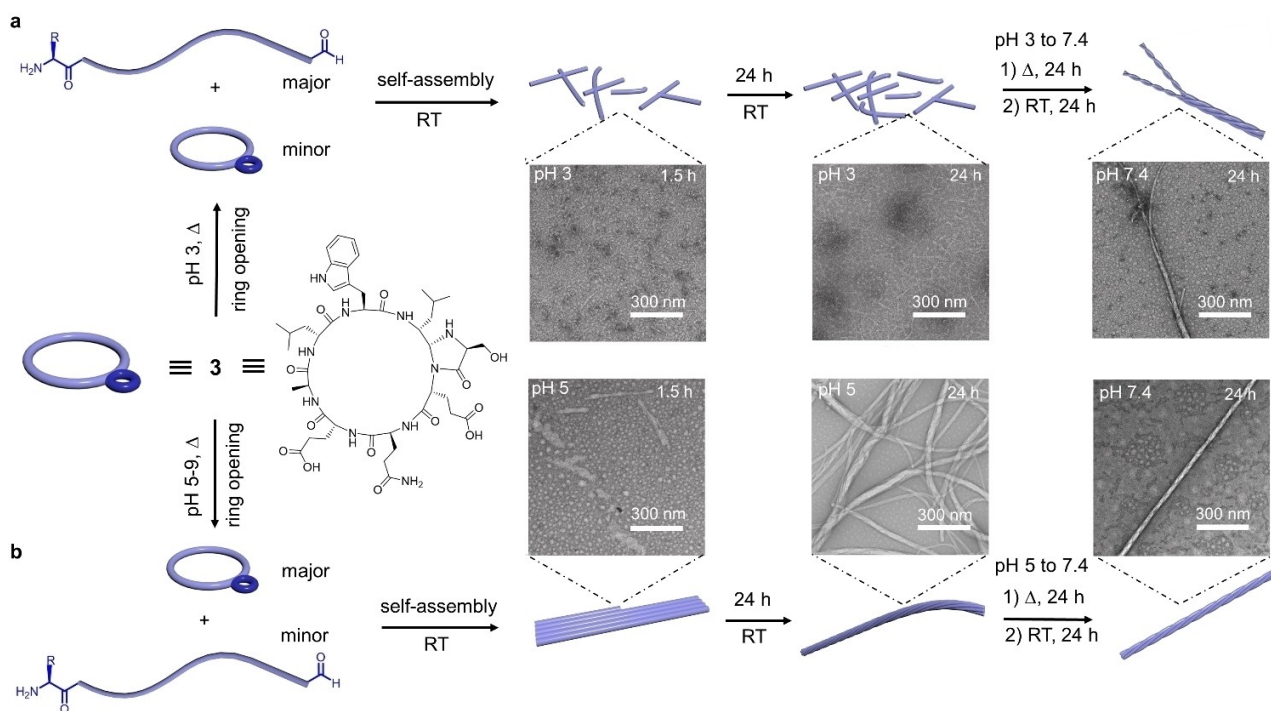


**Figure 4.** a) Schematic illustration of the thermal-induced ring-opening and the self-assembly of **3** (1 mM) at variable pHs, a) at pH 3.0; b) at pH 5.0–9.0. TEM images of **3** after two heating and cooling processes. Firstly, at pH 3.0 (a) or 5.0–9.0 (b), at 68 °C for 24 h, then cooled down to RT (room temperature) and stabilized for 1.5 h (left) and 24 h (middle). Secondly, adjusted the pH to 7.4, then at 68 °C for 24 h followed at RT for 24 h (right).

omers account for 25%. The ratio for the major cyclic isomer is consistent with the ratio (74%) of a linear peptide featuring a C-terminal D-Leu, as evidenced in  $^1\text{H}$  NMR, suggesting an excellent dr. By contrast, the linear peptide **8** with a C-terminal Gly-H afforded a pair of diastereomers **9** in nearly equal ratio when forming the 4-imidazolidinone ring (Figure S42, 43). Overall, these results support that the side chain of the C-terminal amino acid is important for the higher dr in cyclization. To further verify the nucleophilic attack of the amidic nitrogen of the second amino acid (D-Glu) to the preformed imine rather than the side hydroxyl group of the Ser, peptides **20** and **21** were synthesized (For characterizations see Figure S76–79). Peptide **20** with a D-Pro failed (consistent with the results by Raj et al<sup>[15a]</sup>) to cyclize under the identical conditions we used, whereas **21** could cyclize efficiently with a dr value 1:3 (Figure S79).

We next used CD to investigate the influence of the substitutes on the secondary structures. The threonine analogue (**5**) with an extra methyl group showed an identical structural shape with **3** in CD (Figure 5a, b). Compounds **7**, **9**, and **15** displayed a distinct minimum band around 200 nm, indicating that the peptides were less constrained, possibly frequently interchanging between random coil, beta sheet and helical conformation. The loss of distinct secondary structures might be attributed to the mixtures of two diastereomers (inseparable) in **7** and the loss of the chirality at position 8 for **9** and **15**. Compound **11**, with a L-Asn residue, exhibited a distorted spectrum compared to **3** and **5**,

with a lower intensity at 222 nm (Figure 5b). As expected, the introduction of a Trp group (**13**) significantly enhanced the indole stacking (strong negative band at 227 nm), as evidenced in CD spectra.<sup>[29]</sup> The mean residue molar ellipticity did not change for **5** and **7** but showed subtle differences for other analogues when increasing the concentration from 25  $\mu\text{M}$  to 400  $\mu\text{M}$ , suggesting **5** and **7** almost in monomeric state while others show gradual tendency to aggregate (Figure S61). For all the cyclic peptides containing a 4-imidazolidinone ring, no notable difference was observed in their nanostructures by FT-IR. By contrast, the control peptide **15** without the 4-imidazolidinone ring in the backbone showed the presence of absorption at  $1625\text{ cm}^{-1}$  for amide I, which was absent in other peptides, suggesting the  $\beta$ -sheet conformation for **15** (Figure S67).

The subtle difference in the structure also influences the assembly morphology. The nanoribbon arrays formed by **5** and **9** (two isomers being inseparable in HPLC) at 1.5 h gradually coiled to form dominant intertwined nanotubular structures at 24 h (Figure 5c). The dynamic interfibrillar process may undergo individual tubes to fiber bundles, then nanoribbon arrays, further hierarchically intertwined nanostructures transformations. The formation of the nanoribbons may be attributed to the multiple contacts from the backbone amides and the side chains via hydrogen bonding interactions,  $\pi$ - $\pi$  stacking interactions.<sup>[17]</sup> Despite the difficulty of following the transformation from nanoribbons to dominant intertwined nanostructures, it is suspected that the secondary structure (left-handed helices) plays a crucial role

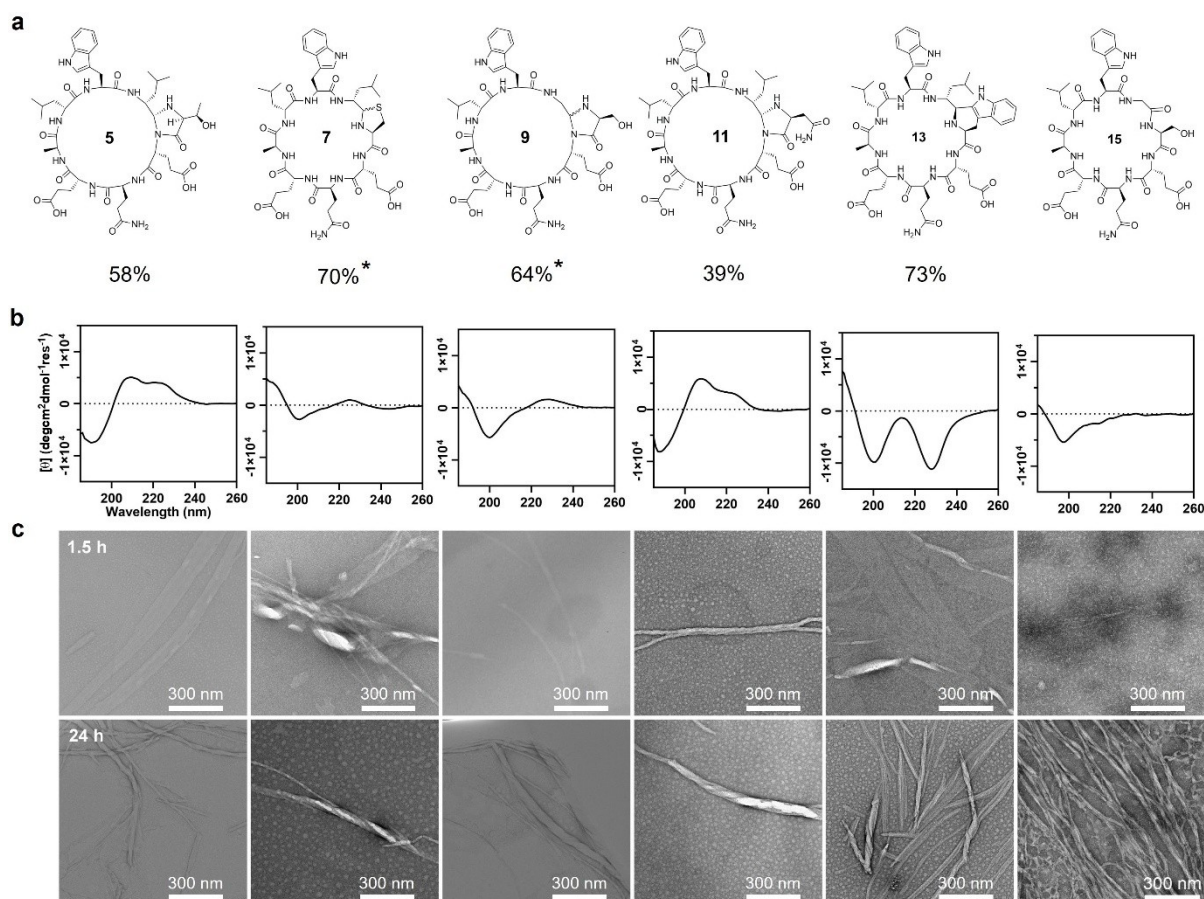


**Figure 5.** Structural and self-assembly comparison of various analogues. a) Chemical structures of other five- and six-membered analogues. The conversion yields to the major isomers are listed below the chemical structures, \* represents the total conversion for two diastereomers. b) CD spectra of the cyclic peptide at 100  $\mu\text{M}$  at pH 7.4 in 10 mM phosphate buffer. c) TEM images showed the time-dependent assembly for cyclic peptides from 1.5 h to 24 h at 1 mM in 10 mM phosphate buffer (pH 7.4). The N and C-terminal residue are labeled as 1 and 8, respectively.

in promoting this transformation in a time dependent mode. Compound **7** presented coiled nanoribbons and wrinkled ribbon arrays reminiscent of unconsolidated nanosheets at 1.5 h. The ribbon arrays could convert to the intertwined coils at 24 h as imaged. The Asn-analogue (**11**) displayed two types of morphologies, namely nanoribbon arrays and intertwined hierarchical structures at 1.5 h, with intertwined hierarchical structures being dominant at 24 h. The polymorphism suggests the complexity and unpredictability within the molecular structure and physicochemical factors driving the self-assembly.<sup>[30]</sup> Besides, the nanoribbon arrays formed by **13** could reach more than 300 nm in width at 1.5 h due to stronger  $\pi$ - $\pi$  interactions, displaying partially intertwined ribbons and taps (Figure 5c). As a control, compound **15** with all amides in the backbone but losing the chirality at position 8 showed less propensity to intertwine compared to peptide **9** with a 4-imidazolidinone ring in the backbone, supporting the importance of five-membered ring in promoting the coils. Besides, compound **23** with a L-Ala in the first residue also showed strong propensity to form intertwined nanostructures, proving the role of 4-imidazolidinone ring in promoting the formation of higher-order nanostructures (Figure S84). In addition, we expanded the

substrate scope by replacing the alanine with a cysteine, which conjugated with a maleimide labeled Cy5.5 (**19**) showing interesting parallel arrangement between filament bundles under microscopy (Figure S74, the intermediates **16–18** are shown in the SI). The intertwined structures were undetected, possibly attributed to the large and hydrophobic group of Cy5.5 causing steric clash between the nanofibers (Figure S75).

## Conclusion

This work presents the design of a cyclic peptide platform with a reversible linkage. The ring-chain tautomerism and self-assembly morphology could be tuned by simply changing the pH in water without producing other chemical waste except water. The cyclic monomers could be accessed from partially or largely epimerized linear peptides with a C-terminal aldehyde due to a self-correcting mechanism. The primary sequence contains multiple stereocenters, and complex side chains are the prerequisites for the chirality correction prior to cyclization. Besides, the cyclization mostly leads to two diastereomers, with the major isomer

exhibiting strong resistance to ring-opening under thermal conditions at neutral pH, whereas the minor isomer could transform into the major isomer via a plausible ring-opening and spontaneous cyclization mechanism. The response of the ring-chain tautomerism to pHs under thermal conditions also affects the folding and unfolding of the hierarchical nanostructures. The ring-chain tautomerism could be tuned multiple times without losing any material. Most importantly, the resulting cyclic peptide initiates the 1D to 2D assembly and then self-assembles to form higher-order coils in left-handedness, proving chirality-induced self-assembly. The extrusion of the first residue (L-Ser) from the backbone due to the formation of a 4-imidazolidinone ring, thereby making the two D-residues (D-Glu and D-Leu) adjacent, which may distort the flat conformation adopted in a classical cyclic D,L peptide. Overall, this work shows that the asymmetrical incorporation of a hetero ring in the backbone of cyclic D,L peptides could promote the formation of intertwined hierarchical nanostructures rather than classical nanotubes or nanosheets. This innovative strategy may guide the development of new cyclic peptides and nanomaterials with various structural and functional features.

### Acknowledgements

This project was supported by the National Key Research and Development Program of China (2022YFB3808300), and the National Natural Science Foundation of China (82022038). This research was supported by Instrumentation and Service Centers for Molecular Science and for Physical Science, respectively, as well as by Biomedical Research Core Facilities at Westlake University. The authors also thank Dr. Xiaohu Miao for the assistance with measurement and data interpretation in WAXS, Dr. Xiaohu Shi, Dr. Huy Hoang (from The University of Queensland) for discussions in NMR data analysis, Dr. Xuejiao Yang, Dr. Yixi Xu for microscopy imaging help. The authors also appreciate the valuable advice provided by Dr. Jeffrey Mak from the University of Queensland for preparing the manuscript.

### Conflict of Interest

The authors declare no conflict of interest.

### Data Availability Statement

The data that support the findings of this study are available from the corresponding author upon reasonable request.

**Keywords:** Asymmetrical Backbone · Cyclic Peptides · Intertwined Nanostructures · Ring-Chain Tautomerism · Self-Assembly

- [1] a) A. Rustom, R. Saffrich, I. Markovic, P. Walther, H.-H. Gerdes, *Science* **2004**, *303*, 1007–1010; b) D. M. Davis, S. Sowinski, *Nat. Rev. Mol. Cell Biol.* **2008**, *9*, 431–436.
- [2] *Introduction to Biotechnology: the Science, Technology and Medical Applications* (Ed.: W. T. Godbey), Woodhead Publishing, London, **2014**.
- [3] a) J. T. Davis, O. Okunola, R. Quesada, *Chem. Soc. Rev.* **2010**, *39*, 3843–3862; b) J. R. Granja, M. R. Ghadiri, *J. Am. Chem. Soc.* **1994**, *116*, 10785–10786.
- [4] Y. Lin, S. Taylor, H. Li, K. A. S. Fernando, L. Qu, W. Wang, L. Gu, B. Zhou, Y.-P. Sun, *J. Mater. Chem.* **2004**, *14*, 527–541.
- [5] R. Duncan, R. Gaspar, *Mol. Pharmaceutics* **2011**, *8*, 2101–2141.
- [6] J. Chen, B. Zhang, F. Xia, Y. Xie, S. Jiang, R. Su, Y. Lu, W. Wu, *Nanoscale* **2016**, *8*, 7127–7136.
- [7] a) X. Xie, T. Zheng, W. Li, *Macromol. Rapid Commun.* **2020**, *41*, 2000534; b) J. Wang, L. Hu, H. Zhang, Y. Fang, T. Wang, H. Wang, *Adv. Mater.* **2022**, *34*, 2104704; c) H. Wang, Z. Feng, B. Xu, *Angew. Chem. Int. Ed.* **2019**, *131*, 10532–10541.
- [8] a) D.-S. Yang, Y.-H. Yang, Y. Zhou, L.-L. Yu, R.-H. Wang, B. Di, M.-M. Niu, *Adv. Funct. Mater.* **2020**, *30*, 1904969; b) A. S. Carlini, R. Gaetani, R. L. Braden, C. Luo, K. L. Christman, N. C. Gianneschi, *Nat. Commun.* **2019**, *10*, 1735.
- [9] a) K. Hu, W. Xiong, C. Sun, C. Wang, J. Li, F. Yin, Y. Jiang, M.-R. Zhang, Z. Li, X. Wang, Z. Li, *CCS Chem.* **2020**, *2*, 42–51; b) A. Fuertes, M. Juanes, J. R. Granja, J. Montenegro, *Chem. Commun.* **2017**, *53*, 7861–7871; c) T. Shimizu, W. Ding, N. Kameta, *Chem. Rev.* **2020**, *120*, 2347–2407; d) N. Rodríguez-Vázquez, R. García-Fandiño, M. Amorín, J. R. Granja, *Chem. Sci.* **2016**, *7*, 183–187; e) J. M. Priegue, I. Louzao, I. Gallego, J. Montenegro, J. R. Granja, *Org. Chem. Front.* **2022**, *9*, 1226–1233; f) R. Chapman, M. Danial, M. L. Koh, K. A. Jolliffe, S. Perrier, *Chem. Soc. Rev.* **2012**, *41*, 6023–6041; g) Q. Song, J. Yang, J. Y. Rho, S. Perrier, *Chem. Commun.* **2019**, *55*, 5291–5294; h) Q. Song, Z. Cheng, M. Kariuki, S. C. L. Hall, S. K. Hill, J. Y. Rho, S. Perrier, *Chem. Rev.* **2021**, *121*, 13936–13995.
- [10] M. R. Ghadiri, J. R. Granja, R. A. Milligan, D. E. McRee, N. Khazanovich, *Nature* **1993**, *366*, 324–327.
- [11] a) C. Yuan, W. Ji, R. Xing, J. Li, E. Gazit, X. Yan, *Nat. Chem. Rev.* **2019**, *3*, 567–588; b) J. Yang, X. Yu, J.-I. Song, Q. Song, S. C. L. Hall, G. Yu, S. Perrier, *Angew. Chem. Int. Ed.* **2022**, *61*, e202115208; c) J. Y. Rho, H. Cox, E. D. H. Mansfield, S. H. Ellacott, R. Peltier, J. C. Brendel, M. Hartlieb, T. A. Waigh, S. Perrier, *Nat. Commun.* **2019**, *10*, 4708; d) S. C. Larnaudie, J. C. Brendel, I. Romero-Canelón, C. Sanchez-Cano, S. Catrouillet, J. Sanchis, J. P. C. Coverdale, J.-I. Song, A. Habtemariam, P. J. Sadler, K. A. Jolliffe, S. Perrier, *Biomacromolecules* **2018**, *19*, 239–247.
- [12] J. E. Becker, R. E. Moore, B. S. Moore, *Gene* **2004**, *325*, 35–42.
- [13] T. Jiao, G. Wu, Y. Zhang, L. Shen, Y. Lei, C.-Y. Wang, A. C. Fahrenbach, H. Li, *Angew. Chem. Int. Ed.* **2020**, *59*, 18350–18367.
- [14] L. R. Malins, J. N. deGruyter, K. J. Robbins, P. M. Scola, M. D. Eastgate, M. R. Ghadiri, P. S. Baran, *J. Am. Chem. Soc.* **2017**, *139*, 5233–5241.
- [15] a) V. Adebomi, R. D. Cohen, R. Wills, H. A. H. Chavers, G. E. Martin, M. Raj, *Angew. Chem. Int. Ed.* **2019**, *58*, 19073–19080; b) R. Wills, V. Adebomi, C. Spancake, R. D. Cohen, M. Raj, *Tetrahedron* **2022**, *126*, 133071.
- [16] a) N. Rodríguez-Vázquez, M. Amorín, I. Alfonso, J. R. Granja, *Angew. Chem. Int. Ed.* **2016**, *55*, 4504–4508; b) J. Montenegro, M. R. Ghadiri, J. R. Granja, *Acc. Chem. Res.* **2013**, *46*, 2955–2965; c) R. J. Brea, C. Reiriz, J. R. Granja, *Chem. Soc. Rev.* **2010**, *39*, 1448–1456.
- [17] a) I. Insua, J. Montenegro, *J. Am. Chem. Soc.* **2020**, *142*, 300–307; b) S. Díaz, I. Insua, G. Bhak, J. Montenegro, *Chem. Eur. J.* **2020**, *26*, 14765–14770.

- [18] A. Méndez-Ardoy, J. R. Granja, J. Montenegro, *Nanoscale Horiz.* **2018**, *3*, 391–396.
- [19] a) T. Golakoti, W. Y. Yoshida, S. Chaganty, R. E. Moore, *J. Nat. Prod.* **2001**, *64*, 54–59; b) J. Jokela, L. Herfindal, M. Wahlsten, P. Permi, F. Selheim, V. Vasconcelos, S. O. Døske-land, K. Sivonen, *ChemBioChem* **2010**, *11*, 1594–1599.
- [20] a) S. Enck, F. Kopp, M. A. Marahiel, A. Geyer, *ChemBioChem* **2008**, *9*, 2597–2601; b) S. Enck, F. Kopp, M. A. Marahiel, A. Geyer, *Org. Biomol. Chem.* **2010**, *8*, 559–563.
- [21] a) J. V. Paukstelis, L. L. Lambing, *Tetrahedron Lett.* **1970**, *11*, 299–302; b) F. Fulop, K. Pihlaja, K. Neuvonen, G. Bernath, G. Argay, A. Kalman, *J. Org. Chem.* **1993**, *58*, 1967–1969; c) L. Lázár, F. Fülöp, *Eur. J. Org. Chem.* **2003**, 3025–3042.
- [22] D. Bermejo-Velasco, G. N. Nawale, O. P. Oommen, J. Hilborn, O. P. Varghese, *Chem. Commun.* **2018**, *54*, 12507–12510.
- [23] S. W. Larsen, M. Sidenius, M. Ankersen, C. Larsen, *Eur. J. Pharm. Sci.* **2003**, *20*, 233–240.
- [24] a) S. I. Al-Gharabli, S. T. A. Shah, S. Weik, M. F. Schmidt, J. R. Mesters, D. Kuhn, G. Klebe, R. Hilgenfeld, J. Rademann, *ChemBioChem* **2006**, *7*, 1048–1055; b) Y. Wu, C. Li, S. Fan, Y. Zhao, C. Wu, *Bioconjugate Chem.* **2021**, *32*, 2065–2072.
- [25] a) H. N. Hoang, C. Y. Wu, T. A. Hill, A. D. de Araujo, P. V. Bernhardt, L. G. Liu, D. P. Fairlie, *Angew. Chem. Int. Ed.* **2019**, *58*, 18873–18877; b) R. W. Newberry, R. T. Raines, *Acc. Chem. Res.* **2017**, *50*, 1838–1846.
- [26] M. Ferstl, A. Strasser, H.-J. Wittmann, M. Drechsler, M. Rischer, J. Engel, A. Goepferich, *Langmuir* **2011**, *27*, 14450–14459.
- [27] K. Koner, S. Karak, S. Kandambeth, S. Karak, N. Thomas, L. Leanza, C. Perego, L. Pesce, R. Capelli, M. Moun, M. Bhakar, T. G. Ajithkumar, G. M. Pavan, R. Banerjee, *Nat. Chem.* **2022**, *14*, 507–514.
- [28] a) V. Castelletto, J. Seitsonen, J. Ruokolainen, I. W. Hamley, *Soft Matter* **2021**, *17*, 3096–3104; b) B. Stuart, *Biological Applications of Infrared Spectroscopy*, Wiley, New York, **1997**; c) I. W. Hamley, *Introduction to Peptide Science*, Wiley & Sons, Inc., Hoboken, **2020**.
- [29] a) S.-J. Choi, W.-J. Jeong, S.-K. Kang, M. Lee, E. Kim, D. Y. Ryu, Y.-B. Lim, *Biomacromolecules* **2012**, *13*, 1991–1995; b) C. E. Dempsey, P. E. Mason, P. Jungwirth, *J. Am. Chem. Soc.* **2011**, *133*, 7300–7303.
- [30] a) F. Wang, O. Gnewou, S. Wang, T. Osinski, X. Zuo, E. H. Egelman, V. P. Conticello, *Matter* **2021**, *4*, 3217–3231; b) L. Pieri, F. Wang, A.-A. Arteni, M. Vos, J.-M. Winter, M.-H. Le Du, F. Artzner, F. Gobeaux, P. Legrand, Y. Boulard, S. Bressanelli, E. H. Egelman, M. Paternostre, *Proc. Natl. Acad. Sci. USA* **2022**, *119*, e2120346119.

Manuscript received: March 8, 2023

Accepted manuscript online: July 6, 2023

Version of record online: July 26, 2023